

Insight into the Growth of Multiple Branched MnOOH Nanorods

Yu Li,^{†,‡} Haiyan Tan,[§] Oleg Lebedev,[§] Jo Verbeeck,[§] Ellen Biermans,[§] G. Van Tendeloo,[§] and Bao-Lian Su^{*,†,‡}

[†]State Key Laboratory of Advanced Technology for Materials Synthesis and Processing, Wuhan University of Technology, 122 Luoshi Road, 430070, Wuhan, Hubei, China, [‡]Laboratory of Inorganic Materials Chemistry (CMI), The University of Namur (FUNDP), 61 Rue de Bruxelles, B-5000 Namur, Belgium, and [§]EMAT, University of Antwerp, 171 Groenenborgerlaan, B-2020 Antwerpen, Belgium

Received January 4, 2010; Revised Manuscript Received April 20, 2010

ABSTRACT: Multiple branched manganese oxide hydroxide (MnOOH) nanorods prepared by a hydrothermal process were extensively studied by transmission electron microscopy (TEM). A model of the branch formation is proposed together with a study of the interface structure. The sword-like tip plays a crucial role for the nanorods to form different shapes. Importantly, the branching occurs at an angle of around either 57° or 123°. Specifically, a (111) twin plane can only be formed at the interface with a 123° angle. The interfaces formed with a 57° angle usually contain edge dislocations. Electron energy loss spectroscopy (EELS) demonstrates that the whole crystal has a uniform chemical composition. Interestingly, an epitaxial growth of Mn₃O₄ at the radial surface was also observed under electron beam irradiation; this is because of the rough purification of the products. The proposed mechanism is expected to shed light on the branched/dendrite nanostructure growth and to provide opportunities for further novel nanomaterial structure growth and design.

Introduction

Branched nanostructures have drawn tremendous attention because of their outstanding structural diversity, physical or chemical properties, and potential device applications originating from their special three-dimensional (3D) structures. Applications are found in areas such as chemical sensors, optics, energy conversion, electronics, catalysts, and medicine.^{1–5} Compared with traditional one-dimensional (1D) nanostructures, the branched 1D nanostructures have no artificial interfaces between each nanostructure and can provide a means for parallel connectivity and interconnection of different functional compositions, which could enhance the device efficiency and even expand their potential applications. A popular way to control the synthesis of branched structures is by a multistep strategy such as vapor–liquid–solid (VLS)^{6,7} and solution–liquid–solid (SLS)^{8,9} processes. Another common process uses surfactants as capping agents or soft templates in a solution system to synthesize branched nanostructures.^{10–12} Other methods such as chemical beam epitaxy (CBE) in two steps, electrochemical deposition, redox reaction in aqueous solution and the use of supercritical carbon dioxide have been developed recently.^{13–16} Though many strategies have been explored to synthesize various branched 1D nanostructures, the development of a strategy or a process that is cheap with a facile operating method which has the potential to be scaled up is still of great importance. Furthermore, understanding the formation mechanism of the branched nanostructure remains another burning issue to be solved.

Manganese oxides present very interesting chemical, electrochemical, and physical properties and can be used as magnetic materials, molecular sieves, batteries, and catalysts.^{17–20} Many methods based on conventional solution phase routes have been carried out to synthesize nanostructured crystalline

manganese oxides, such as chemical bath deposition, sol–gel technique, and hydrothermal or solvothermal synthesis.^{21–25} It has been suggested that the properties of these types of materials strongly depend on their crystal structure, specific surface area, bulk density, dimensions, and morphology.^{26–29} Recently, much research has been focused on the synthesis of different morphologies and phases of manganese oxides.^{30–39} Among the manganese oxide compounds, manganese oxide hydroxide (MnOOH) is currently arousing much attention,^{25,40–42} because it has extraordinary adsorption capacities; it is a useful tool for removing many trace elements from aquatic environments.^{43–45} Moreover, it can be easily transformed into several different manganese oxide structures, such as Mn₃O₄, MnO₂, and Mn₂O₃.^{46–52} However, branched MnOOH has seldom been reported, and the formation mechanism remains unknown.^{53,54} As understanding the growth mechanism and shape guiding process is essential for predicting and controlling the final architectures, it is necessary to get insight into the formation mechanism of these types of branched nanostructures.

Transmission electron microscopy (TEM) techniques are critical for structure characterization, especially for nanostructure characterization. In this work, we use TEM to clearly identify the initial step in the growth of multiple branched MnOOH nanorods. Since the branched structures have a typical sword-like shape at the tips/ends, it is expected that this material has specific properties. Hence, conventional transmission electron microscopy (CTEM), high resolution transmission electron microscopy (HRTEM), scanning transmission electron microscopy (STEM), and electron energy loss spectroscopy (EELS) have been used to thoroughly characterize the morphology, the structure, and composition of the material, in order to shed light on the formation and properties of the branched MnOOH nanorods and to provide a new route for the growth and design of novel nanomaterial structures.

*Author to whom correspondence should be addressed. E-mail: baoliansu@whut.edu.cn; tel: 00 86 27 87 66 52 57; or e-mail: bao-lian.su@fundp.ac.be; tel: 00 32 81 72 45 31; fax: 00 32 81 72 54 14.

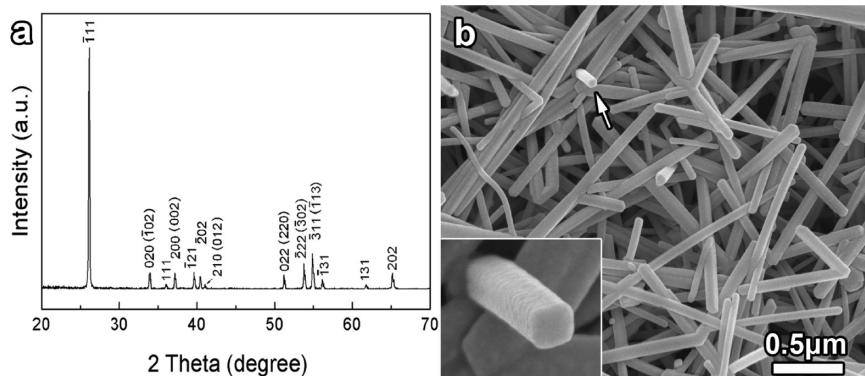


Figure 1. The XRD result (a) and the SEM image of the as-prepared material at a reaction time of 12 h (b). The inset in (b) is an enlarged SEM image of the nanorod indicated by the arrowhead, which shows a regular shape of the nanorod cross section.

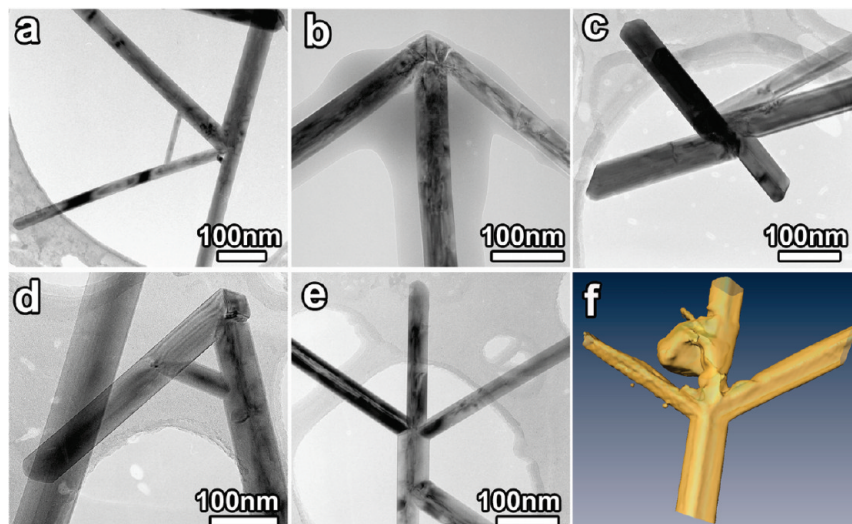


Figure 2. (a–e) The low magnification TEM images of the branched MnOOH nanorods with different shapes. (f) 3D electron tomography reconstruction of the branched nanorods prepared at 2 h. All the branches are approximately in the same plane and the angles between them are around 123° or 57° . The outside faces are concluded to be $\{\bar{1}11\}$ planes. It also shows the rectangular cross section of the rod.

Experimental Section

Synthesis. All the chemical reagents were purchased from Aldrich and were used as received. For a typical synthesis, 0.105 g (0.005 mol) of KMnO_4 was completely dissolved in 50 mL of distilled water to form a purple black solution. Five milliliters of PEG200 (polyethylene glycol, average molecule weight 200) was then added to the solution and it was stirred for 20 min at room temperature until a uniform solution was formed. The obtained uniform solution was put into a 60 mL Teflon-lined stainless steel autoclave, which was subsequently sealed and maintained at 160°C for 12 h, then allowed to cool to room temperature. Next, the as-formed precipitate in the autoclave was filtered then washed with ethanol and water several times. Finally, the obtained precipitate was dried in air at 40°C for 12 h.

Characterization

X-ray diffraction patterns (XRD) were obtained with a Panalytical X'Pert diffractometer using $\text{Cu K}\alpha$ radiation ($\lambda = 1.54056 \text{ \AA}$). Selected area electron diffraction (SAED) was performed on a Philips CM20 microscope. High resolution transmission electron microscopy (HRTEM) was performed on a JEOL 4000EX operating at 400 kV. High angle annular dark field scanning transmission electron microscopy (HAADF-STEM) and scanning transmission electron microscopy with electron energy loss spectroscopy (STEM-EELS)

were performed on a JEOL 3000F at 300 kV. The EELS spectra were acquired by a Gatan GIF2000 1K Phosphor system operating with energy dispersion of 0.3 eV/channel and an approximate energy resolution of 1 eV. 2D scan spectra were recorded in STEM mode with a collection angle of 28.6 mrad and a convergence angle of 10 mrad. Recording time for each spectrum was 5 s. EELSMODEL was used to extract the O/Mn atomic ratio of the recorded spectra.

Results and Discussion

XRD analysis was primarily used to determine the structure of the as-synthesized material (Figure 1a). All the peaks can be attributed to the monoclinic structure of MnOOH with SG $P2_1/c$ (No. 14) and lattice parameters $a = 0.5299 \text{ nm}$, $b = 0.5270 \text{ nm}$, $c = 0.5299 \text{ nm}$, $\beta = 114.37^\circ$. They are consistent with the structure data from JCPDS No. 88-0649. The morphology is investigated by scanning electron microscopy (SEM) (Figure 1b). Figure 1b shows that the product is one-dimensional MnOOH nanorods, which clearly displays the branched structure. A view along the length direction of one stretched out nanorod indicates the rectangular form of each nanorod. CTEM and SEM observations revealed that in the as-prepared material about 80% of the nanorods have a branched structure. Most of the nanorods had a diameter

ranging from 50 to 90 nm with a high aspect ratio as shown in Figure 2a–e. The two-dimensional (2D) projections reveal that multiple branching regularly occurs with special shapes such as an arrowhead (Figure 2b), a fan blade shape

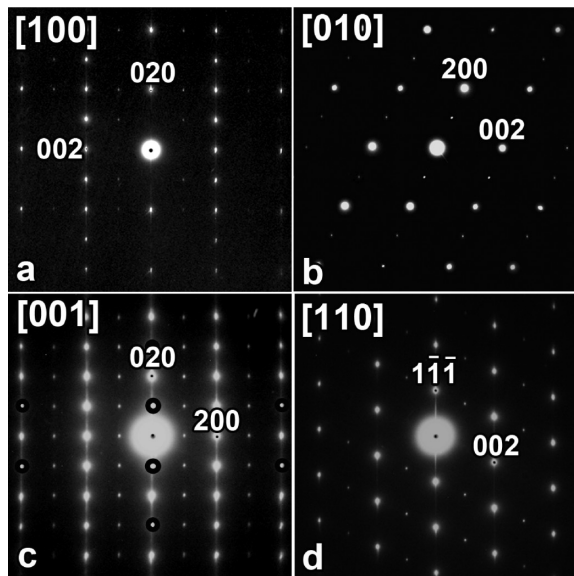


Figure 3. (a–d) The electron diffraction patterns of the as-prepared MnOOH nanorods along the main zone axes. They are indexed with SG $P2_1/c$ and parameters $a = 0.530$ nm, $b = 0.528$ nm, $c = 0.530$ nm, and $\beta = 114.38^\circ$.

(Figure 2c), or a capital letter A (Figure 2d). The connections at the junction can be clearly observed, which suggests that the branches are formed through self-assembly of 1D nanorods. Along the length direction, the branches have a uniform and constant size. Most of the tips/ends of the 1D nanorods are not flat but have a sword-like shape. Very interestingly, one observes that the branches have a constant angle of around 60° or 120° with respect to each other. This has been confirmed by electron tomography. Using electron tomography, we have reconstructed the 3D shape of the branched nanorods (Figure 2f). It shows that all branches are lying in the same plane. The side surface is proved to be $\{1\bar{1}1\}$ by the dimensional measurement of the reconstructed image, which presents $\{1\bar{1}1\}$ surface planes and shows an abrupt thickness change at the projection.

Selected area electron diffraction (SAED) was carried out to characterize the structure of the as-prepared branched nanorods. It shows that all the straight nanorods are single crystal and the diffraction patterns can be indexed to the monoclinic structure of MnOOH, consistent with the XRD results (Figure 1a). The SAED patterns along the main zone axes [100], [010], [001], and [110] are presented in Figure 3. Note that the [001] ED pattern contains reflections due to double diffraction (circled spots in Figure 3c). Apart from these double diffraction spots, the pattern is similar to the [100] ED pattern (Figure 3a). The elongations of the diffraction spots and the streaking, particularly in the [001] zone, are caused by the high aspect ratio of the branched nanorods.

Figure 4a demonstrates a branched MnOOH nanorod with four branches labeled as B1, B2, B3, and B4. The projected

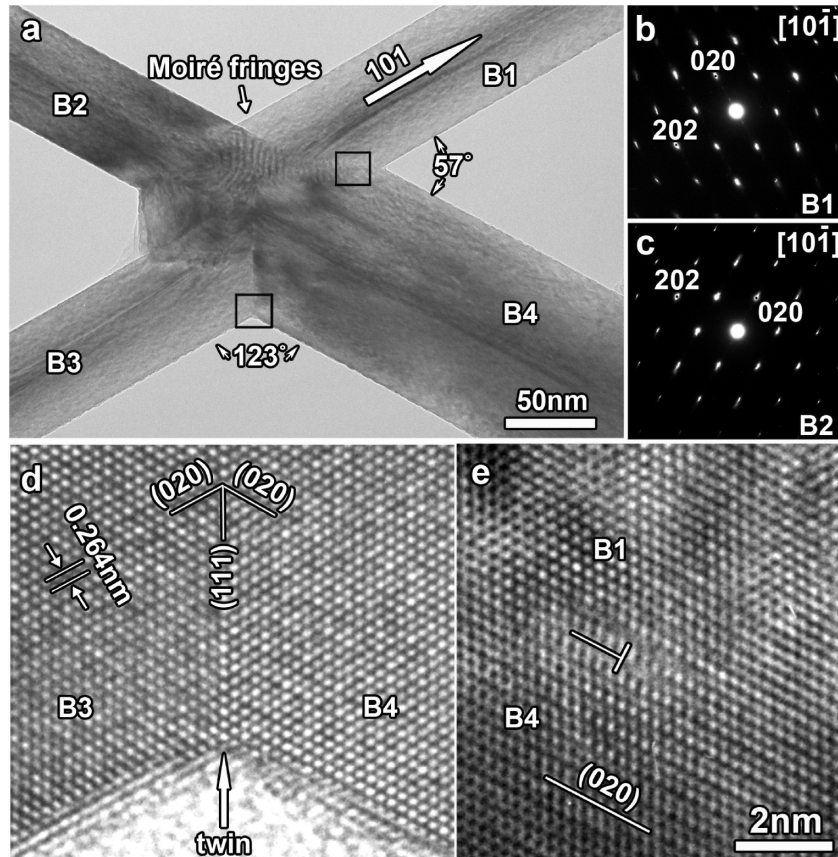


Figure 4. TEM images of a four branched nanorod and the corresponding SAED patterns of the sample prepared at 12 h. (a) Low magnification TEM image to show the morphology of the branch with its SAED patterns of branch B1 (b) and B2 (c). (d) HRTEM image of the interface region (lower rectangle region) between branch B3 and B4, which clearly shows a (111) twin plane at the interface. (e) HRTEM image of the interface between branches B1 and B4, which clearly shows an edge dislocation with a slide plane (010).

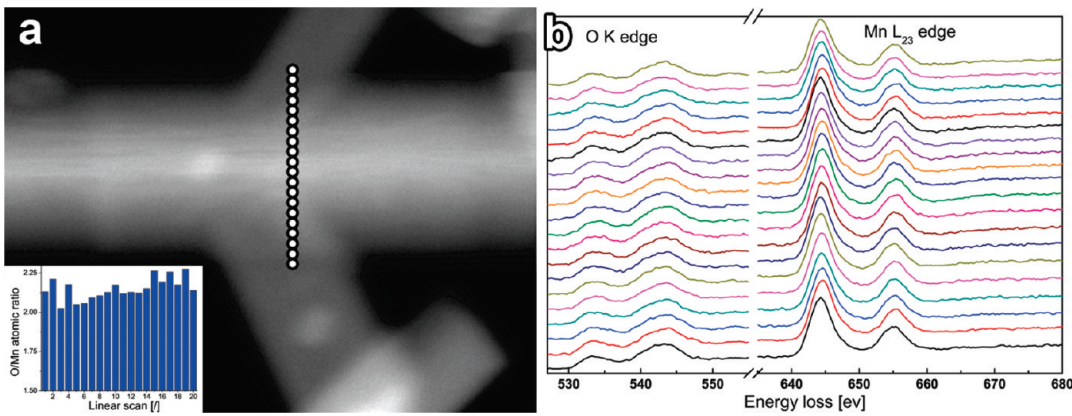


Figure 5. (a) HAADF STEM image and (b) the EELS spectra from a linear scan in the branched region. The dots in (a) indicate the probe position of the scan and the inset of (a) is the O/Mn atomic ratio. The EELS spectra do not show significant change in shapes and peak positions.

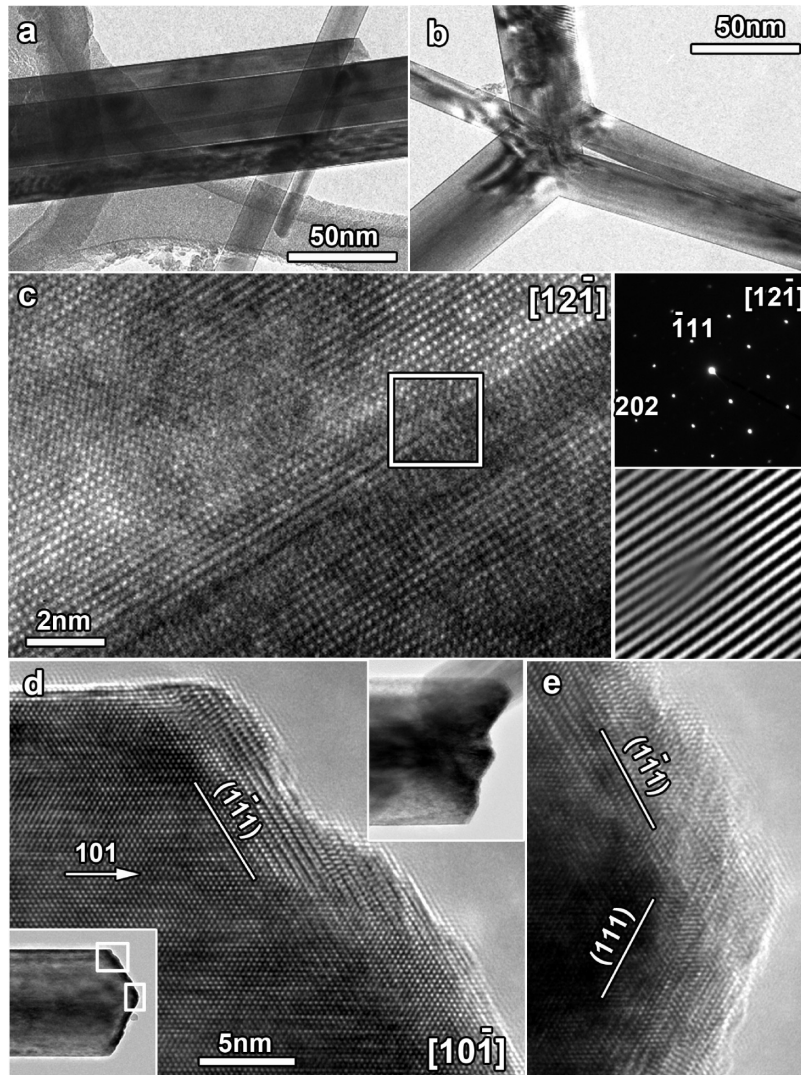


Figure 6. TEM images of the sample prepared at 2 h. (a) The small rods orientated combine with each other and start to grow as one bigger straight nanorod. (b) A branched structures are formed. (c) HRTEM image of the merging rods which is similar with what is shown in (a). The right-up figure shows its ED pattern and the right lower one is a FFT that shows the edge dislocation at the $(\bar{1}11)$ plane. Panels (d) and (e) are HRTEM images of the sword tip shown in the inset at the left side. The exposed growth plane is (111) . The inset at the right up side of (d) also shows the (111) exposed plane with a tooth shape.

angles are 57° between B1–B4 and 123° between B3–B4, respectively. The SAED patterns (Figure 4b,c) were taken

from branches B1 and B2, respectively. Both patterns can be indexed as the $[10\bar{1}]$ zone but rotated 57° with respect to each

other. The ED patterns of B3 and B4 are the same as that of B1 and B2 (patterns not shown). Therefore, B3 has the same orientation as B1, and B4 has the same orientation as B2. The fact that all four branches show the same [101] zone orientation confirms the fact that all branches are lying in the same plane and suggests that they have an epitaxial relationship where B1 and B3 are rotated 57° with respect to B2 and B4. It also implies that the growth direction of the nanorods is along [101], in agreement with the elongation of the (perpendicular) 001 reflections in Figure 3. In the middle of Figure 4a, branches B2 and B1 partially overlap. Therefore, some broad fringes, known as Moiré fringes, are observed with a separation of (3.9 ± 0.5) nm. The same is observed at the interface between B1 and B4 but not between B3 and B4. The presence of Moiré fringes indicates either a slight rotation of the lattice or a small difference in interplanar spacing along the particular [101] direction. From the SAED patterns of branches B1 and B2, it can be concluded that the Moiré fringes result from the overlap of the (020) and the (111) lattice fringes. The measured Moiré fringe spacing is in agreement with the calculated one, based on the monoclinic structure of MnOOH.

HRTEM was applied to carefully examine the branched structure and particularly the connecting interfaces. The high resolution image of the B3–B4 interface (Figure 4d) clearly displays twinning along the common (111) plane (indicated by the arrowhead), with the (020) planes of the MnOOH structure making an angle of 123°. The (111) twin plane forms a 61.5° angle with the (020) planes of both variants, in agreement with the orientation from the SAED patterns (Figure 4b, c). The atomic model (shown further in Figure 7) is also in agreement with this 123° angle. However, HRTEM observations reveal that not all branches connect through the formation of twin interfaces. For example, no twinning is observed at the interface between B1–B2 (Figure S1 in Supporting Information) and the interface between B1–B3. Figure 4e reveals detailed information of the interconnection between B1–B4, formed at the angle of 57°. A different mechanism is playing here: the (111) planes of B1 connect to the (020) planes of B4. Edge dislocations are resulting because of the (slight) difference in lattice spacing between both families (Figure 4e).

STEM-EELS spectra of the nanorods are acquired at different positions at the branched region (Figure 5a). No significant differences were found between these spectra (Figure 5b). The EELSMODEL⁵⁵ fitting gives an O/Mn atomic ratio of 2.15(7) at the branched region. The atomic ratio and variation are the same as those measured from a single nanorod. It indicates that we have a uniform MnOOH chemical composition at the branch region.

To gather more information on the formation mechanism, a study on the crystal growth evolution process was carried out. SEM observations demonstrated that small 1D nanorods form after 30 min of reaction through the coalescence of existing single crystal nanoparticles, which are generated at the beginning of the reaction (about 5 min). As the reaction time continues, the nanorods become larger and longer and branched nanorods appear after 1 h reaction. After a reaction time of 12 h, about 80% of the products are branched nanorods (Figure S2 and S4 in Supporting Information). Figure 6 shows representative TEM images of a sample synthesized at 2 h. Figure 6a illustrates how the large 1D nanorods are formed as a result of the oriented assembling of several small nanowires along their side surfaces thus reducing the surface energy. Note that the three small rods in Figure 6a have the same diffraction contrast, which implies the three

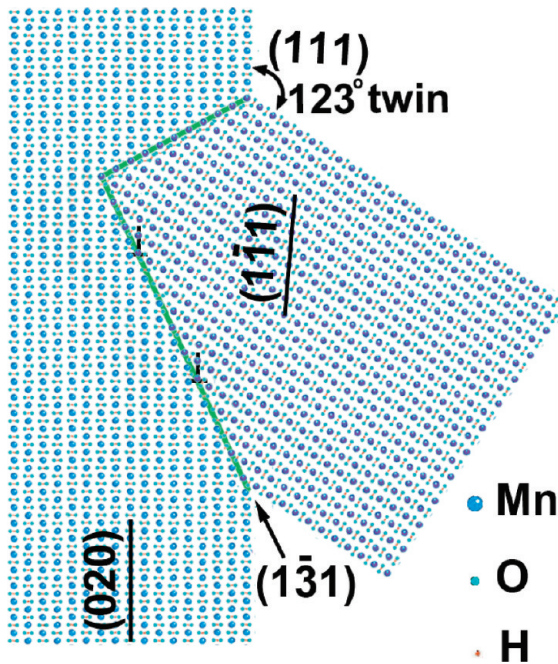


Figure 7. The atomic arrangements of the branched nanorod formation with the (111) twin plane and the edge dislocation along the (010) plane at the interface. The (13̄1) plane is the arrangement of dislocations.

rods are in the same crystal orientation. The small gaps in between will be rapidly filled by later growth, and eventually some edge dislocations may be introduced to compensate for slight misorientations (Figure 6c). This HRTEM image together with the FFT (right lower corner) clearly shows the presence of a dislocation. It also demonstrates that the oriented attachment grows along the (111) crystal plane with eventually edge dislocations along the interface. The growth along the length direction is so fast that they soon grow into a single rod with a uniform lateral size (Figure S5 in Supporting Information). Another possible way to reduce the surface energy is to attach the active tip/end surfaces with one another leading to the formation of branched structures (Figure 2). When these small rods are self-assembling and form branched structures as in Figure 6b, some gaps may be left; these however will be filled soon. In fact, all the exposed sword-like tips/ends of the nanorods are potential active sites. Prolonging the reaction time ultimately leads to more multiple branched nanorods. HRTEM of the tip/end of a sword-like nanorod (Figure 6d,e) reveals that the exposed planes during growth are the {111} planes. The very tip of the nanorod is not always very well crystallized immediately after formation (Figure 6e). A detailed atomic arrangement of the branches is presented in Figure 7. The tip plane (111) of one vertical nanorod attaches with the tip (111) plane of another nanorod. Since both planes are exactly the same, twinning occurs at the (111) plane with an angle of 123°. At the other side of this junction however, the crystal structure does not fit perfectly and therefore edge dislocations are formed to form a low angle grain boundary.

On the basis of these experimental results, the formation mechanism of the branched MnOOH nanorods can be proposed as follows from the SEM and TEM observations (Figure 8). In the very beginning, the concentration of reactants is comparatively high; therefore, some nuclei can be formed very fast resulting in the occurrence of single crystal nanoparticles in the system according to our experimental

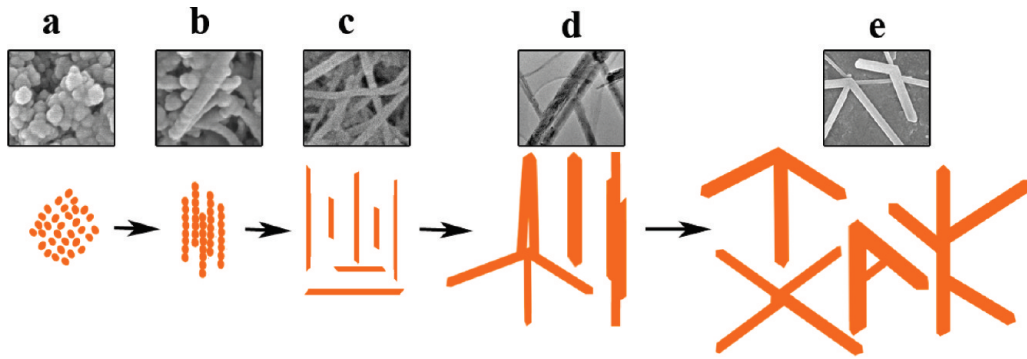


Figure 8. Schematic illustration of the formation stages of different shapes of the branched MnOOH nanorods.

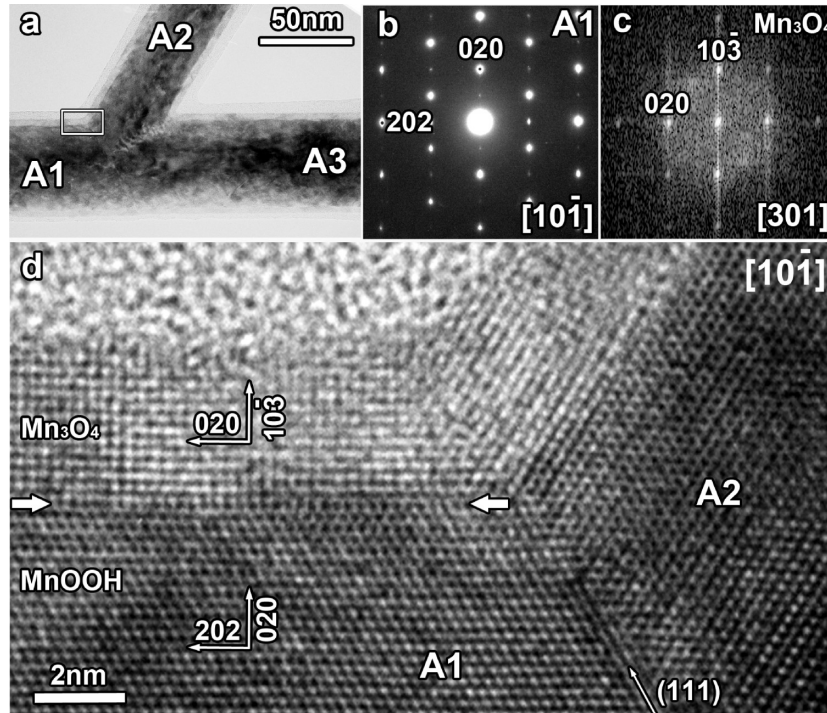


Figure 9. TEM images and SAED patterns of the epitaxial growth on the surface of three branched nanorods prepared at 12 h. (a) Low magnification of the nanorods at the $[10\bar{1}]$ direction. (b) SAED patterns of branch A1; note that some extra reflection spots are present such as 101 and 010 spots here. (c) FFT of the epitaxial grown region on the surface of branch A1, which only presents the 010 and 101 spots in (b). It can be indexed by the $[301]$ ED pattern of the Mn_3O_4 structure. (d) The HRTEM image at the crossover of branches A1 and A2. Each branch has an epitaxial grown Mn_3O_4 layer along the 010 direction of MnOOH that is 4 nm in thickness. The opposite arrowheads indicate the beginning atoms layer of the epitaxial growth.

results (Figure 8a). The nanoparticles orient to form one-dimensional nanorods (Figure 8b) and grow fast along the $[101]$ direction to form small 1D nanorods with sword-like tips/ends (Figure 8c). Through oriented attachment along the $\{111\}$ side surfaces of the small 1D nanorods, the 1D nanorods increase their diameter to become bulky rods (from 30 to 90 nm, Figure S3 in Supporting Information). At the same time, the tips/ends of some small 1D nanorods can attach to the exposed sword-like sites of other 1D nanorods resulting in the appearance of branched nanorods (Figure 8d). These single and branched nanorods keep growing and relaxing their defects inside to minimize the surface energy. Finally, multiple branched nanorods with different shapes arise (Figure 8e). It is necessary to note that the steps c, d, and e can practically occur simultaneously and are separated just for convenient explanation. If the tips/ends of those 1D nanorods join in parallel to the sword-like sites of other 1D nanorods or

the branched nanorods, a twin plane forms with an angle of 123° . If two branches are slightly misoriented upon joining, pure twinning cannot appear even if the two branches form an angle around 123° ; this is, for example, the case for branch B2 growing from the middle section of branch B1 in Figure 4. The growth of the junction in Figure 4 can then be imagined as follows: branch B3 self-assembles and attaches its tip (111) plane to the top-left side tip $(1\bar{1}\bar{1})$ plane of a bigger branch B4 through twinning. Since branch B4 is larger, its active growth plane is only partially connected with branch B3. When another branch B1 approaches to the top-right side active tip plane $(1\bar{1}1)$ of branch B4, a connection is made at an angle of 57° formed through the introduction of edge dislocations to overcome the mismatch at the junction. This case happens between branch B1 and branch B2 also, resulting in an oriented attaching at the middle sites of the branch B1 and growth from the jointing sites. Generally, both the twin plane

growth and the presence of edge dislocations often occurs owing to an oriented attachment at the interface to reduce the surface energy and to match the bond lengths between the branches.^{56–58}

Under the electron beam irradiation during TEM observations, epitaxial growth of a second phase can be observed along the radius of the nanorods (Figure 9). The thickness of the epitaxial layer is usually 4–5 nm. From the bright field image at low magnification, one can notice that there are actually two thin layers at the surface of the nanorods with a lighter contrast (Figure 9a). The outer one is an amorphous layer and the inner layer is a crystalline layer (Figure 9d). Comparing the [101] SAED pattern of the branch A1 (Figure 9b) with the clean [101] ED pattern of Figure 4b,c, some weak extra reflections are present in the ED pattern of the branch A1; they are originating from the epitaxial layer. The local FFT of the epitaxial layer is shown in Figure 9c. This FFT cannot be indexed based on the MnOOH structure, but it can be indexed as the [301] pattern of the Mn₃O₄ tetragonal structure with SG *I4₁/amd* (No. 141) and lattice parameters *a* = 0.576 nm and *c* = 0.944 nm. The epitaxial growth occurs along the (020) plane of MnOOH with the epitaxial relationship MnOOH (020)/Mn₃O₄ (103) and MnOOH [202]//Mn₃O₄ [020]. There is almost no lattice mismatch at the interface since both the interplanar spacings of (101) MnOOH and (020) Mn₃O₄ are 0.288 nm. Generally, this kind of epitaxial growth should be a kinetically controlled process. This epitaxial growth behavior is to be expected for a product prepared from a solution phase synthesis. When the final product is not thoroughly purified, unreacted reactant precursors are left absorbed on the surface of the product. Under vacuum conditions, the energy provided by the electron beam allows the chemical reagents to react, resulting in epitaxial growth at the surface.

Conclusion

Multiple branched MnOOH nanorods were extensively characterized by TEM, HRTEM, STEM, EELS, and electron tomography. A formation mechanism has been proposed according to these investigations. The first nanorods originate from the nanoparticles formed at the beginning of the reaction, which grow along the [101] direction to form small 1D nanorods with a sword-like tips. The oriented attachment of the {111} planes of some small 1D nanorods allow the rods to grow larger. 1D nanorods also attach to each other by their sword-like tips in order to form branched nanorods. The shape of the branches depends on the growth speed and the size of the branches. The branches form either by twinning along the (111) plane, forming 123° branches, or the introduction of edge dislocations to match the slight mismatch. As the reaction time is extended, more and more multiple branched nanorods with different shapes appear, owing to the contribution of exposed sword-like sites. The unreacted chemical reagents adsorbed on the surface of the nanorods can cause the epitaxial growth of Mn₃O₄ along the radius of the nanorods under electron beam irradiation. These results are expected to provide rational strategies in nanomaterial synthesis and nanostructure design.

Acknowledgment. This work was realized in the frame of an Interuniversity Attraction Poles Program (Inanomat-P6/17)-Belgian State-Belgian Science Policy and the project “Redugaz”, financially supported by the European community

and the Wallon government in the frame of Interreg IV (France-Wallonie). B.L.S. acknowledges the Chinese Central Government for an “Expert of the State” position in the program of “Thousand talents” and the Chinese Ministry of Education for a Changjiang Scholar position at the Wuhan University of Technology. H.T. acknowledges the financial support from FWO-Vlaanderen (Project no. G.0147.06). J.V. thanks the financial support from the European Union under Framework 6 program for Integrated Infrastructure Initiative, Reference 026019 ESTEEM.

Supporting Information Available: Figures of SEM observations of the samples at different reaction times and HRTEM images. This information is available free of charge via the Internet at <http://pubs.acs.org/>.

References

- (1) Qin, Y.; Wang, X. D.; Wang, Z. L. *Nature* **2008**, *451*, 809.
- (2) Tang, Z. Y.; Kotov, N. A.; Giersig, M. *Science* **2002**, *297*, 237.
- (3) Huang, M. H.; Mao, S.; Feick, H.; Yan, H. Q.; Wu, Y. Y.; Kind, H.; Weber, E.; Russo, R.; Yang, P. D. *Science* **2001**, *292*, 1897.
- (4) Cui, Y.; Liber, C. M. *Science* **2001**, *291*, 851.
- (5) Milliron, D. J.; Hughes, S. T.; Cui, Y.; Manna, L.; Li, J.; Wang, L.-W.; Alivisatos, A. P. *Nature* **2004**, *430*, 190.
- (6) Dick, K. A.; Deppert, K.; Larsson, M.; Martensson, T.; Seifert, W.; Wallenberg, L. R.; Samuelson, L. *Nat. Mater.* **2004**, *3*, 380.
- (7) Zhu, J.; Peng, H.; Marshall, A. F.; Barnett, D. M.; Nix, W. D.; Cui, Y. *Nat. Nanotechnol.* **2008**, *3*, 477.
- (8) Trentler, T. J.; Hickman, K. M.; Goel, S. C.; Viano, A. M.; Gibbons, P. C.; Buhro, W. E. *Science* **1995**, *270*, 1791.
- (9) Holmes, J. D.; Johnston, K. P.; Doty, R. C.; Korgel, B. A. *Science* **2000**, *287*, 1471.
- (10) Peng, Z. A.; Peng, X. G. *J. Am. Chem. Soc.* **2002**, *124*, 3343.
- (11) Yin, Y.; Alivisatos, A. P. *Nature* **2005**, *437*, 664.
- (12) Hsu, Y.-J.; Lu, S.-Y. *Small* **2008**, *4*, 951.
- (13) Suyatin, D. B.; Sun, J.; Fuhrer, A.; Wallin, D.; Froberg, L. E.; Karlsson, L. S.; Maximov, I.; Wallenberg, L. R.; Samuelson, L.; Hu, H. Q. *Nano Lett.* **2008**, *8*, 1100.
- (14) Ma, Y. Y.; Jiang, Z. Y.; Kuang, Q.; Zhang, S. H.; Xie, Z. X.; Huang, R. B.; Zheng, L. S. *J. Phys. Chem. C* **2008**, *112*, 13405.
- (15) Yu, H.; Wang, D.; Han, M. Y. *Adv. Mater.* **2008**, *20*, 2276.
- (16) Cao, F.; Liu, Y.; Hu, W.; Chen, Q. *J. Phys. Chem. C* **2008**, *112*, 2337.
- (17) Brock, S. L.; Duan, N.; Tian, Z. R.; Giraldo, O.; Zhou, H.; Suib, S. L. *Chem. Mater.* **1998**, *10*, 2619.
- (18) Tarascon, J. M.; Armand, M. *Nature* **2001**, *414*, 359.
- (19) Ammundsen, B.; Paulsen, J. *Adv. Mater.* **2001**, *13*, 943.
- (20) Winter, M.; Brodd, R. J. *Chem. Rev.* **2004**, *104*, 4245.
- (21) Kijlstra, W. S.; Daamen, J.; Vandegraaf, J. M.; Vanderlinde, B.; Poels, E. K.; Bliek, A. *Appl. Catal., B* **1996**, *7*, 337.
- (22) Lei, S.; Tang, K.; Fang, Z.; Zheng, H. *Cryst. Growth Des.* **2006**, *6*, 1757.
- (23) (a) Yuan, Z. Y.; Zhang, Z.; Du, G.; Ren, T. Z.; Su, B. L. *Chem. Phys. Lett.* **2003**, *378*, 349. (b) Yuan, Z. Y.; Ren, T. Z.; Du, G.; Su, B. L. *Chem. Phys. Lett.* **2004**, *389*, 83.
- (24) Zhang, W.; Yang, Z.; Liu, Y.; Tang, S.; Han, X.; Chen, M. *J. Cryst. Growth* **2004**, *263*, 394.
- (25) Hu, C. -C.; Wu, Y. -T.; Chang, K.-H. *Chem. Mater.* **2008**, *20*, 2890.
- (26) Bach, S.; Henry, M.; Baffier, N.; Livage, J. *J. Solid State Chem.* **1990**, *88*, 325.
- (27) Pistoia, G.; Antonini, A.; Zane, D.; Pasquali, M. *J. Power Sources* **1995**, *56*, 37.
- (28) Hill, L. I.; Verbaere, A.; Guyomard, D. *J. Power Sources* **2003**, *119*, 226.
- (29) Sugantha, M.; Ramakrishnan, P. A.; Hermann, A. M.; Warmsingh, C. P.; Ginley, D. S. *Int. J. Hydrogen Energy* **2003**, *28*, 597.
- (30) Han, X. G.; Jin, M. S.; Kuang, Q.; Zhou, X.; Xie, Z. X.; Zheng, L. S. *J. Phys. Chem. C* **2009**, *113*, 2867.
- (31) Ding, Y. -S.; Shen, X. -F.; Gomez, S.; Luo, H.; Aindow, M.; Suib, S. L. *Adv. Funct. Mater.* **2006**, *16*, 549.
- (32) Ould-Ely, T.; Prieto-Centurion, D.; Kumar, A.; Guo, W.; Knowles, W. V.; Asokan, S.; Wong, M. S.; Rusakova, I.; Lutte, A.; Whitmire, K. H. *Chem. Mater.* **2006**, *18*, 1821.
- (33) Giraldo, O.; Brock, S. L.; Marquez, M.; Suib, S. L.; Hillhouse, H.; Tsapatsis, M. *Nature* **2000**, *405*, 38.

- (34) Zitoun, D.; Pinna, N.; Frolet, N.; Belin, C. *J. Am. Chem. Soc.* **2005**, *127*, 15034.
(35) Yuan, J.; Laubernds, K.; Zhang, Q.; Suib, S. L. *J. Am. Chem. Soc.* **2003**, *125*, 4966.
(36) Zhong, X. H.; Xie, R. G.; Sun, L. T.; Lieberwirth, I.; Knoll, W. *J. Phys. Chem. B* **2006**, *110*, 2.
(37) Wu, C.; Xie, Y.; Wang, D.; Yang, J.; Li, T. *J. Phys. Chem. B* **2003**, *107* (13), 583.
(38) Li, Z.; Ding, Y.; Xiong, Y.; Yang, Q.; Xie, Y. *Chem. Commun.* **2005**, 918.
(39) Zheng, Y.; Cheng, Y.; Bao, F.; Wang, Y.; Qin, Y. *J. Cryst. Growth* **2006**, *286*, 156.
(40) Zhang, Y.; Liu, Y.; Guo, F.; Hu, Y.; Liu, X.; Qian, Y. *Solid State Commun.* **2005**, *134*, 523.
(41) Sun, X.; Ma, C.; Wang, Y.; Li, H. *Inorg. Chem. Commun.* **2002**, *5*, 747.
(42) Zhou, F.; Zhao, X.; Yuan, C.; Xu, H. *J. Mater. Sci.* **2007**, *42*, 9978.
(43) Chiu, V. Q.; Hering, J. G. *Environ. Sci. Technol.* **2000**, *34*, 2029.
(44) McKenzie, R. M. *Aust. J. Soil Res.* **1980**, *18*, 61.
(45) Bochatay, L.; Persson, P.; Sjöberg, S. *J. Colloid Interface Sci.* **2000**, *229*, 584.
(46) Zhang, Y. C.; Qiao, T.; Hu, X. Y. *J. Solid State Chem.* **2004**, *177*, 4093.
(47) Folch, B.; Larionova, J.; Guari, Y.; Guérin, C.; Reibel, C. *J. Solid State Chem.* **2005**, *178*, 2368.
(48) Zhang, Y. C.; Qiao, T.; Hu, X. Y.; Zhou, W. D. *J. Cryst. Growth* **2005**, *280*, 652.
(49) Xi, G.; Peng, Y.; Zhu, Y.; Xu, L.; Zhang, W.; Yu, W.; Qian, Y. *Mater. Res. Bull.* **2004**, *39*, 1641.
(50) Du, G. H.; Yuan, Z. Y.; Van Tendeloo, G. *Appl. Phys. Lett.* **2005**, *86*, 063113.
(51) Zhang, Z.; Zhang, Y.; Zhang, W.; Wang, X.; Qian, Y. T.; Wen, X.; Yang, S. *J. Solid State Chem.* **2006**, *179*, 679.
(52) Dong, X. Y.; Zhang, X. T.; Liu, B.; Wang, H. Z.; Li, Y. C.; Huang, Y. B.; Du, Z. L. *J. Nanosci. Nanotechnol.* **2006**, *6*, 818.
(53) Zheng, D.; Yin, Z.; Zhang, W.; Tan, X.; Sun, S. *Cryst. Growth Des.* **2006**, *6*, 1733.
(54) Mi, Y.; Zhang, X.; Yang, Z.; Li, Y.; Zhou, S.; Zhang, H.; Zhu, W.; He, D.; Wang, J.; Van Tendeloo, G. *Mater. Lett.* **2007**, *61*, 1781.
(55) (a) Bertoni, G.; Verbeeck, J. *Ultramicroscopy* **2008**, *108*, 782. (b) Verbeeck, J.; Bertoni, G. *Ultramicroscopy* **2008**, *108*, 74. (c) Verbeeck, J.; Van Aert, S.; Bertoni, G. *Ultramicroscopy* **2006**, *106*, 976. (d) Verbeeck, J.; Van Aert, S. *Ultramicroscopy* **2004**, *101*, 207.
(56) Penn, R. L.; Banfield, J. F. *Science* **1998**, *281*, 969.
(57) Portehault, D.; Cassaignon, S.; Baudrin, E.; Jolivet, J. P. *J. Mater. Chem.* **2009**, *19*, 7947.
(58) Fanfair, D. D.; Korgel, B. A. *Chem. Mater.* **2007**, *19*, 4943.